Understanding the influence of initial cluster size distribution on crystallization dynamics in phase-change materials

A. Aladool[2], M. M. Aziz[1], and C. D. Wright[1]

[1]College of Engineering, Mathematics and Physical Sciences, University of Exeter, Exeter EX4 4QF, United Kingdom

[2]Department of Mathematics, College of Education for Pure Science, University of Mosul, Iraq

Abstract

Phase-change materials are recognized as major technological contenders for the development of fast, low power and small non-volatile memories, and for realising the evolutionary paradigm of simultaneous data processing and storage for brain-like and neural computing. The (re)crystallization process remains to be the limiting factor in deciding the operating speeds of phase-change devices. It has been shown experimentally that pre-annealing amorphous phase-change materials leads to shorter crystallization times and therefore increased device switching speeds. This has been attributed to the formation of nano-clusters embedded in the amorphous phase that reduce the incubation time for nucleation and leads to faster crystallization. Recent work using enhanced transmission microscopy has confirmed the formation of nuclei that are few nanometres in size which enhance the crystallisation speed. However, the correlation between the initial size distribution of nano-clusters on the crystallization dynamics is still uncertain, which is crucial for increasing the speed in phase-change memories and data processors. This work aims to simulate the distribution of cluster sizes following pre-annealing and melt-quenching in as-deposited amorphous phase-change materials using the Master rate equation approach. Moreover and to use this approach to systematically investigate the effects of theses simulated and theoretical Gaussian initial clusters densities in the sub-nanometre to few tens of nanometres range on the crystallization dynamics in phase-change material at different annealing rates. This investigation revealed the enhancement of crystallization speeds with narrow initial distributions of small cluster sizes of few nanometres, for the same initial crystalline concentration, in agreement with enhanced microscopy observations.

1. Introduction

The inception and development of phase-change materials for memory applications in both the optical and electronic domains[1] has paved the way for significant advances in material compositions, and realising the evolutionary paradigm of simultaneous data processing and storage for brain-like and neural computing.[2,3,4] In particular, phase-change materials demonstrated excellent device scalability down to single nanometre dimensions,[5,6] ultra-fast switching speeds (picoseconds to nanosecond range)[7], ultra-low power consumption,[5,6] multilevel operation,[8] good data retention (10 years at 110 °C),[9] and excellent endurance (up to 10^{12} cycles).[9]

The memory and processing capabilities of phase-change materials such as the well known $Ge_2Sb_2Te_5$ material (referred to as GST thereafter) are created through changes in their optical and electrical properties. These changes result from the transformation between the crystalline and amorphous phases of the material triggered mostly thermally using either optical or electrical excitations, with sufficient optical or electrical contrast between the two phases and their intermediate levels to enable detection and processing. The phase transformation in phase-change materials from the initial amorphous phase often starts with the formation of nuclei, which then grow and consequently crystallize the material. Controlling and reducing the crystallization time during the writing and erasing stages is critically important for the development of high-speed, low-power phase-change processors and memories. Moreover, repeated writing, erasing and pre-annealing (priming) causes microstructural changes to the starting amorphous phase leading to deviation and drift in their optical and electrical properties compared to the as-deposited case, which impacts their operation and performance.

Experimental studies using static laser testers on thin GST films (25-70 nm thick) indicated reduction of the crystallization times from hundreds of nanoseconds in the as-deposited state, to tens of nanoseconds in the melt-quenched or pre-annealed state (at temperature below the crystallization temperature).[10,11] These effects were attributed to the formation of nano-crystal nuclei which greatly reduce the time for the formation of critical crystals, therefore increasing the nucleation rate and reducing crystallization time.

Thus pre-pulse annealing (using electrical pulses) is employed as a strategy to reduce the crystallization time in GST films in phase-change random access memories (PCRAM).[7] More recently and to elucidate the nature and sizes of these nano-clusters, statistics-based detection using fluctuation transmission electron microscopy (FTEM) and high-resolution TEM (HRTEM) experimental studies have revealed that thermal treatment of GST films using temperatures lower than the crystallization temperature can indeed increase the number and size of crystalline clusters embedded in the amorphous phase.[12,13,14] The size of these clusters were in the range 2-8 nm.

There is still however a lack of a fundamental understanding of the cluster size distributions resulting from the various thermal treatments that phase-change material undergo during operation, and the influence of the resulting initial cluster size distributions on the crystallization dynamics (crystallization time and temperature) during annealing at low and high heating rates. Hence in this article, the effects of a variety of initial cluster size distributions on the crystallization dynamics of an initially amorphous GST phase-change material is studied theoretically at different heating rates using the physically realistic and computationally efficient Master rate equation method. The simulated initial states include the as-deposited, melt-quenched, and pre-annealed states expected in practical device operations. To gain a more comprehensive understanding of the influence of a wider range of potential initial cluster size distributions, theoretical Gaussian initial cluster size distributions with different cluster size means, widths and densities is implemented in the Master rate equation simulations. The simulated and assumed initial cluster size densities are then used as initial conditions for transient crystallization simulations in the Master rate equation to study the correlation between initial cluster size density and crystallization dynamics in phase-change materials.

The Master rate equation method models both nucleation and growth by the attachment and detachment of monomers,[15] yielding transient cluster size distributions in the sub-critical and super-critical regimes under isothermal and non-isothermal annealing conditions.[16,17] Hence this physically realistic simulation method was used to understand the effects of viscosity on reaction rates and crystallization speed in phase-change materials, and extract pertinent kinetic parameters from calorimetric measurements.[18]

Moreover, various cluster size distributions can be specified as initial conditions in this model to describe the initial state of the phase-change material for further crystallization simulations. Hence the Master rate equation model is ideally suited for studying the transient and non-uniform evolution of clusters of different sizes under different heat treatments in phase-change materials and their influence on the crystallization dynamics.

2. Master rate equation simulations

The fundamental theories of cluster formation dynamics and complete theoretical development of the Master rate equation used in this work are described in detail in [18]. For convenience and ease of reference to the terms used in the theoretical simulations, the Master rate equation is rewritten here as:

$$\frac{dZ(n,t)}{dt} = f(n-1,t,T)Z(n-1,t) + g(n+1,t,T)Z(n+1,t) - f(n,t,T)Z(n,t) - g(n,t,T)Z(n,t),\ n \geq 2 \tag{1}$$

describing the transient evolution of clusters Z of size n monomers per unit volume with temperature T. $f(n,t,T)$ and $g(n,t,T)$ are the attachment and detachment rates respectively, and dependant on the work needed for cluster formation including the surface and bulk free energies.[18] The physically realistic, non-Arrhenius MYEGA viscosity model was adopted in the Master rate model in this work as described in [18]. The volume fraction of crystallised material χ is then computed from summation of the cluster size densities produced from the solution of (1) at a given instant of time using:

$$\chi = \sum_{n=2}^{n_{\max}} nZ(n,t)/Z_0 \tag{2}$$

where Z_0 is total monomer density of the starting (amorphous) phase.

The Master rate equation in (1) represents a system of coupled system of n equations, which was solved numerically for the cluster size distribution $Z(n,t)$ using the *ode*15s solver in Matlab, subject to an initial cluster size distribution and using absolute and relative tolerances of 10^{-10} (to provide convergence to a stable and accurate solution with practical simulation time). The solver tracks the formation and destruction of clusters of size $n \geq 2$ ($n = 1$ representing the amorphous phase) in response to temperature changes. The initial starting states considered in this work include the as-deposited, melt-quenched, and pre-annealed states. The as-deposited state refers to the initially amorphous phase with no pre-existing nuclei. This is easily modelled in the Master rate equation as an initial and uniform cluster size density of $Z(n,0) = 10^{-11}$ clusters/m^3, and will be used throughout this paper to describe the as-deposited state. The implementation of the melt-quenched and the pre-annealed initial states will be described in the next sections of this article.

Following the implementation of the initial cluster size distribution in the Master rate equation, numerical simulations of crystallization are performed by application of ramped and uniform temperatures according to $T = T_0 + \phi t$ where T_0 = 300 K is room temperature, t is the time and ϕ is the constant heating rate. The two heating rates of 50 K/s and 40,000 K/s applied in the simulations in this work correspond to heating rates that can be achievable using ultrafast calorimetry experiments,[19,20] and enable comparison with measurements of crystallization dynamics at different annealing conditions. The maximum number of equations (upper limit of cluster size) was considered assuming a circular geometry for clusters in the size range 2-8 nm[11,12,13] corresponding to approximately 10-40 monomers. However to account for volumetric distributions and larger clusters, a maximum size of 200 monomers (corresponding to few tens of nanometres) is used in the simulations that follow. The phase-change material parameters used in the simulations are listed in Table I,[18] and correspond to the well-known GST composition.

Table 1 Thermodynamic and kinetic parameters for the GST material used in the Master rate equation numerical simulations

Parameter	Value	unit
Volume of a monomer	2.9×10^{-28} [a]	m^3
Enthalpy of fusion	6.18×10^{8} [a]	J/m^3
Melting temperature	889 [b]	K
Specific surface energy	0.066 [c]	J/m^2
Wetting angle	100 [d]	deg
Glass transition temperature	383 [e]	K
Infinite temperature viscosity	1×10^{-5} [f]	(Pa.s)
Fragility index	47 [g]	
Viscosity activation energy	1.76±0.05 [h]	eV

[a] References [17] and [21]

[b] Reference [22]

[c] Reference [23]

[d] Reference [17]

[e] References [19], [24], [25], and [26].

[f] Extrapolated from Reference [19] for $T > T_m$.

[g] Reference [27]

[h] Reference [28] for temperatures below the glass transition temperature.

2.1. Melt-quenching simulations

Melt-quenching occurs repeatedly during the writing and erasure processes in phase-change memories and processors to arrive at the amorphous starting phase for subsequent annealing operations. Thus it is of interest to study the resulting cluster size distributions following this operation and how they affect the crystallization speed when the material is subsequently recrystallized. Obtaining a melt-quenched amorphous state requires that the applied temperature in the GST material exceeds the melting point of 889 K, followed by cooling at high rates to quench the melted region into the amorphous state. Typical cooling rates required for re-amorphization of GST are of the order of tens of degrees per nanosecond.[29]

Melt-quenching is simulated here at three different cooling rates to determine the appropriate cooling rate at which the crystalline volume fraction is minimum. Starting with the fully crystalline material, a constant temperature of 885 K (sufficiently close but lower than the melting point for GST - therefore within the limit of applicability of the bulk free energy term for cluster formation in [18]) was initially applied in the simulations for a very short period of time (5 ns chosen here) to enable dissociation of monomers and simulate melting. This is followed by linear cooling down to room temperature over the three time durations of 1 ns, 10 ns, and 100 ns (corresponding to the cooling rates 676 K/ns, 67.6 K/ns, and 6.76 K/ns respectively) as shown in Figure 1(a). Figure 1(b) shows the corresponding calculated crystalline volume fractions, with the minimum fraction obtained at steady-state when the cooling time is 1 ns.

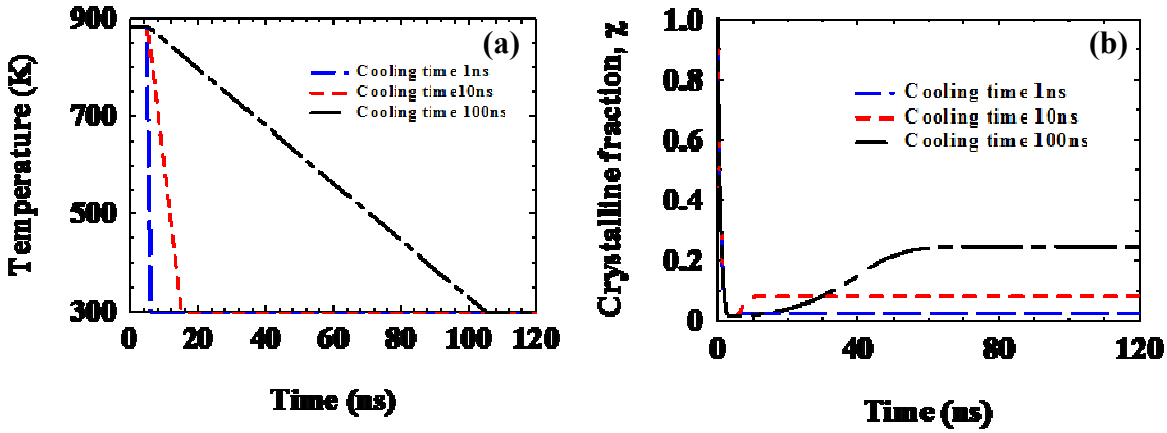

Figure 1(a) Temperature profile in the melt-quench simulations with three different cooling times to room temperature. (b) Transient crystallization curves following the application of the temperature profiles in (a). The steady-state crystalline fraction (blue line) at the cooling time of 1 ns is 0.0266.

Figure 2(a) shows the steady-state cluster size distributions produced from the simulations for the three cooling times, illustrating the very narrow distribution of smaller clusters at the lowest cooling time of 1 ns, consistent with the lowest crystalline volume fraction. For the longest cooling time of 100 ns, there is a wider distribution of cluster sizes including small and large cluster leading to the largest crystalline volume fraction in Figure 1(b) (red line). Figure 2(b-d) are graphic illustrations of a random distribution of the steady-state cluster sizes in the simulation space corresponding to the curves in (a) for the three different cooling times. Figure 2(b) shows the formation of only small clusters of few monomers due to the short cooling time, while longer cooling times permit the growth of larger clusters in Figure 2(c) and (d) leading to the increased crystalline volume fractions shown in Figure 1(b).[14] It is noted that the same cluster size distributions and

corresponding volume fractions obtained upon melting and cooling from the initial crystalline phase in Figure 1 and Figure 2, can also obtained by annealing an initially amorphous material to 885 K followed by cooling at the same rates. The three quantifiable cluster size distributions resulting from the melt-quenching simulations are used next as initial states in crystallization simulations at different heating rates.

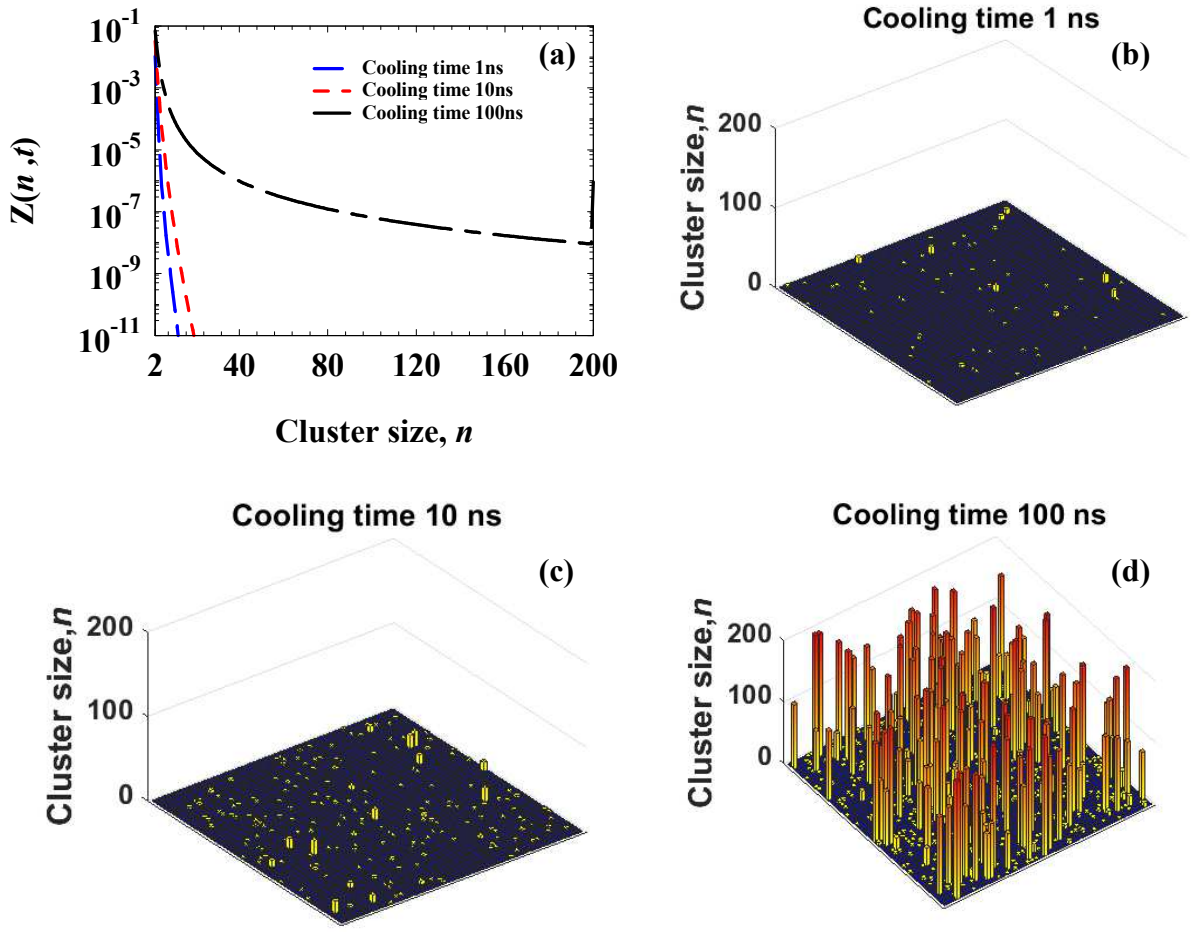

Figure 2(a) Steady-state cluster size distribution following the melt-quench simulations for three different cooling times. (b) - (d) Three-dimensional plots depicting the steady-state cluster sizes in the simulation spaces for the three cooling times of 1 ns, 10 ns, and 100 ns respectively. Note: The three-dimensional plots have been converted from the vector one-dimensional plots in (a) to a two-dimensional, arbitrary space of cluster size height matrix for illustration.

Figure 3 illustrates the calculated crystalline volume fractions in the Master rate equation using the melt-quenched cluster size distributions in Figure 2(a) as initial conditions, and compared to the as-deposited (amorphous) state. At longer cooling times following melting, the existence of a wide distribution of large clusters increases the initial

crystalline volume fraction and naturally reduces the crystallization temperature (defined as the temperature where the crystallization rate is maximum). With reduced cooling time from the melt in the initial cluster distribution, the resulting crystallization temperature increases towards the as-deposited value due to the narrow distribution of very small clusters embedded in the amorphous state. These observations were found to be applicable to the 50 K/s heating rate (Figure 3(a) and (b)) and to the 40,000 K/s heating rate (Figure 3(c) and (d)) as well. Thus the melt-quenching simulations indicate that cooling rates in the 10s and 100s of K/ns are sufficient to produce a very narrow distribution of very small clusters, closely approaching the as-deposited amorphous state with negligible effect on subsequent crystallization.

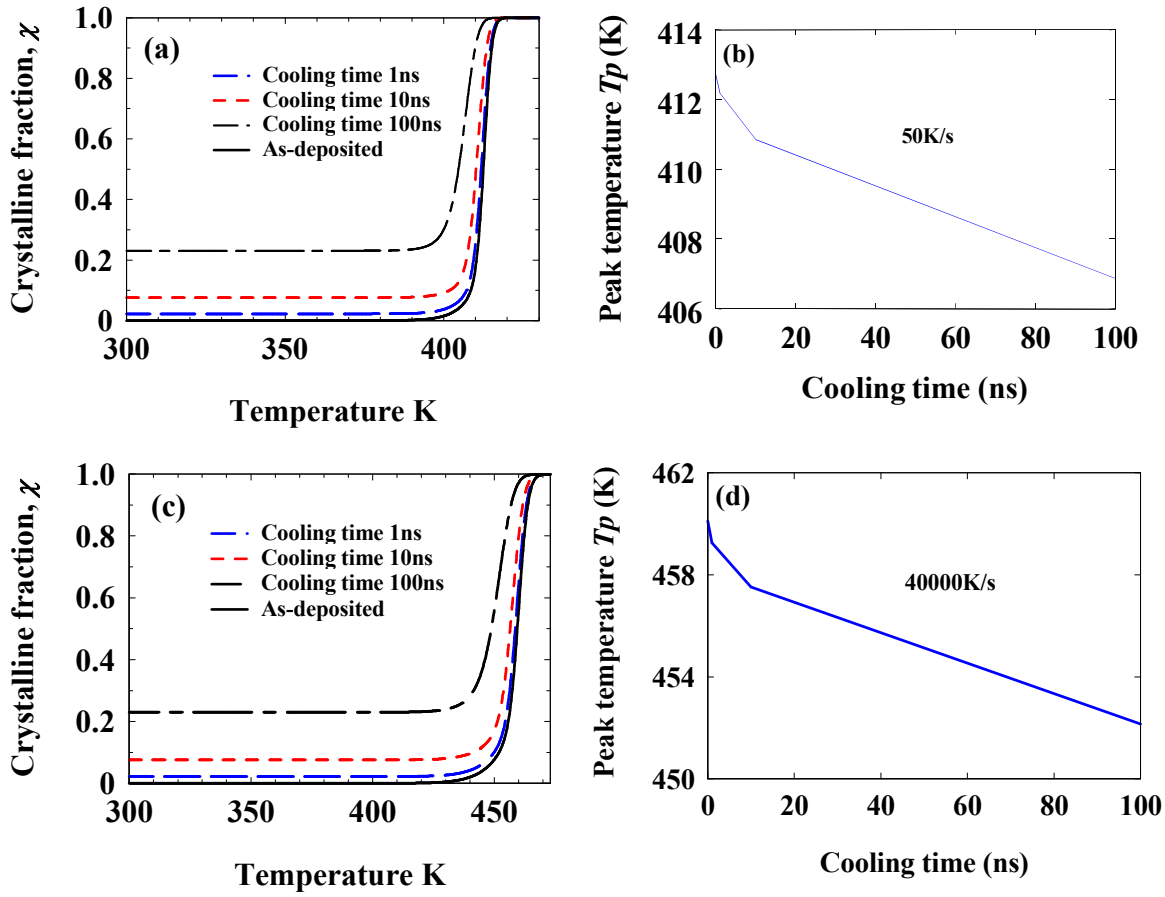

Figure 3 Calculated crystalline volume fraction as a function of temperature during ramped anneals at two different heating rates with three different melt-quenched initial state (a) 50K/s. (c) 40,000K/s. (b) and (d) Peak temperature, T_p as a function of cooling time, determined from the 1st derivatives of the crystalline fraction curves in (a) and (c), indicating that reducing cooling time can lead to decrease peak (crystallization) temperature.

2.2. Pre-annealing simulations

In this section, practical pre-annealing treatments at temperatures well below the crystallization temperature for GST are considered to investigate the effects of the different resulting initial amorphous states on crystallization dynamics. Moreover, theoretical initial distributions are also investigated that are not necessarily produced by the thermal treatments above, assuming Gaussian distributions with different cluster size means and widths spanning the entire range of cluster sizes (up to 200 monomers or few tens of nanometres), which are then used in crystallization simulations at different heating rates.

2.2.1. Practical pre-annealing simulations

The as-deposited amorphous material is heated here using ramped annealing to temperatures well below the crystallization temperature, to study the resulting steady-state cluster size distributions and use them as initial state for transient crystallization simulations under ramped annealing conditions. The pre-annealing simulation is carried out by applying a temperature ramp in the range 300-353 K, which is lower than the reported crystallization temperatures for GST thin-films (~403-423 K),[12,30] with a relatively low heating rate of 0.033 K/s (to ensure that nucleation will take place in the simulation and to allow comparison with published high-resolution TEM imaging of nano-clusters). Figure 4 plots the calculated steady-state pre-annealed cluster size distribution (blue line), and compares it to the as-deposited distribution (red line). This figure shows that pre-annealing at this heating rate produces a large density of smaller cluster sizes up to 20 monomers, a low concentration of larger clusters with almost uniform distribution, and a very narrow distribution of large clusters of 200 monomers in size, embedded in the parent amorphous phase. It is interesting to note that the size of the dominant smaller clusters (up to 20 monomers) obtained from the simulations agrees with the experimentally observed nano-cluster sizes of 5-8 nm for GST using high-resolution TEM under the same pre-annealing condition.[12,13,14]

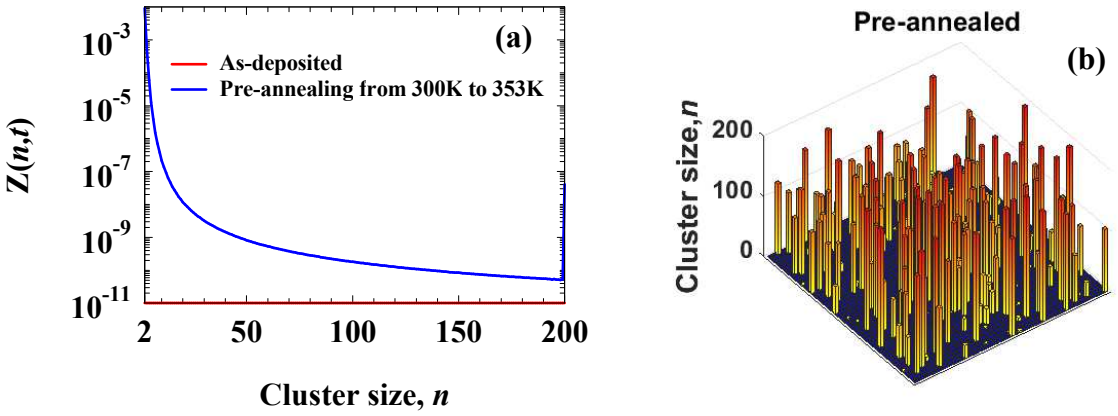

Figure 4 (a) As-deposited and pre-annealed cluster size distribution following ramped annealing in crystallization simulations to a temperature 353 K (well below the crystallization temperature for GST). (b) Visual representation of the steady-state cluster size distribution following pre-annealing in (a) (blue curve).

The pre-annealed cluster size distribution in Figure 4(a) was used as the initial state for transient crystallization simulations using the Master rate equation with ramped annealing at heating rates of 50 K/s and 40,000 K/s. The simulations yielded the crystalline volume fractions shown in Figure 5. As indicated in this figure, the effect of the pre-annealed initial cluster size distribution in this case is to slightly increase the initial crystalline volume fraction, and slightly reduce the crystallization temperature and crystallization time compared to the as-deposited state. This is due to the existence of nucleation centres from pre-annealing that enhances nucleation and subsequent growth. The change in crystallization temperature is better illustrated using the time derivative of the crystalline volume fractions shown in Figure 5(b) and (d).

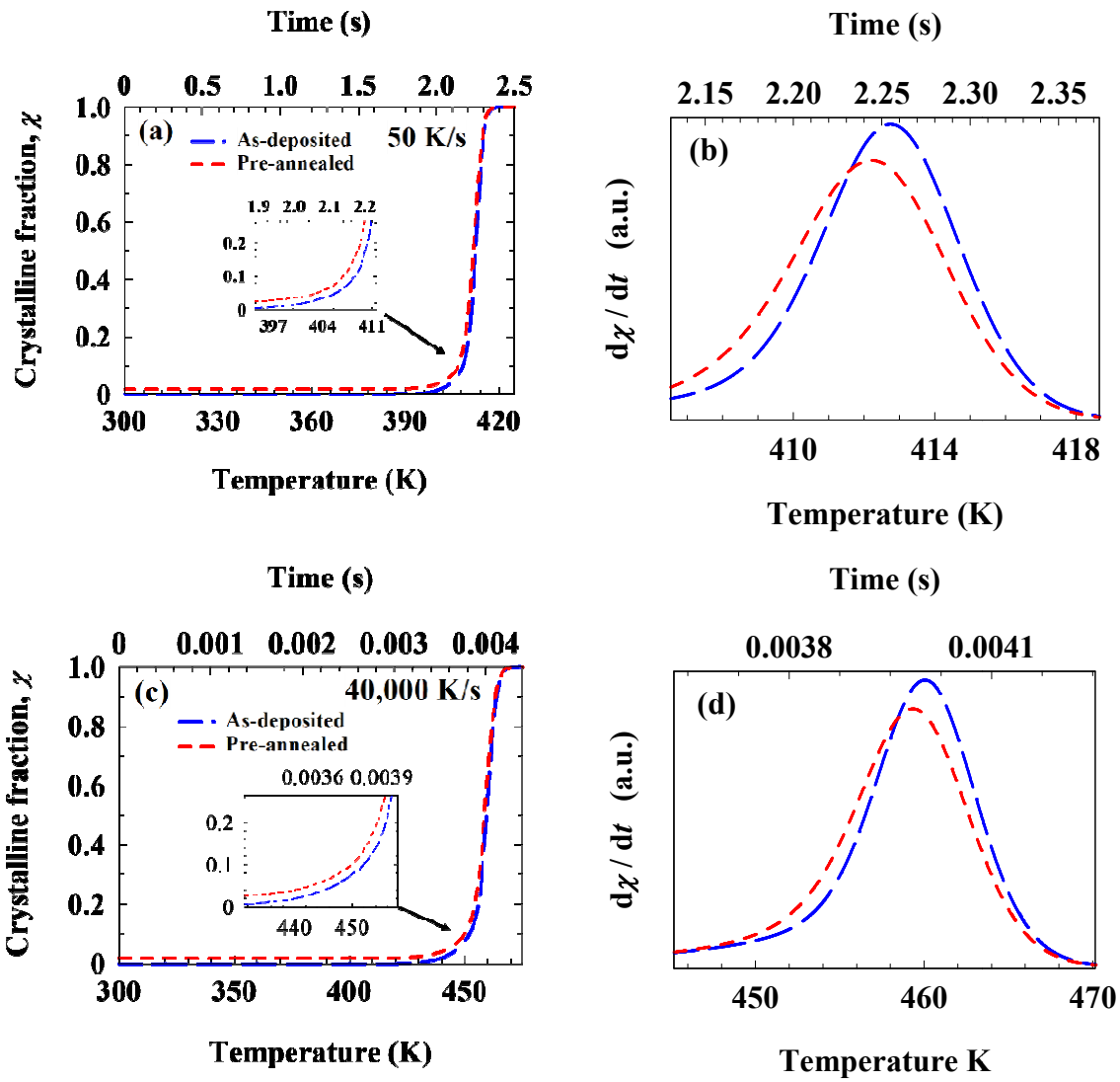

Figure 5 Calculated crystalline volume fraction as a function of temperature during ramped annealing at two different heating rates with the pre-annealed initial state: (a) 50 K/s heating rate and (b) corresponding crystallization rates. (c) 40,000 K/s heating rate and (d) corresponding crystallization rates. The peaks of the crystallization rate plots determine the peak crystallization temperature.

To understand the crystallization curves in Figure 5, the corresponding transient cluster density changes are illustrated in Figure 6 for a selection of cluster sizes at the heating rates of 50 K/s and 40,000 K/s for the as-deposited (dashed lines) and pre-annealed (solid lines) states. This figure shows non-uniform nucleation for the different cluster sizes, with smaller clusters (e.g. n = 3) in the as-deposited state requiring longer time to be formed, which consequently delays the formation and growth of larger clusters as illustrated by the dashed lines in Figure 6. The existence of a distribution of smaller cluster from pre-annealing (e.g. n = 3), on the other hand, speeds up the formation of larger clusters through the attachment of monomers and therefore reduces the crystallization time (compared to the as-deposited state) as shown by the solid lines in Figure 6. The larger

remaining clusters have almost uniform distribution in the density plot in Figure 4(a), and grow at nearly the same rate as the smaller clusters leading to the relatively small overall increase in the cyrstallization rate of the material.

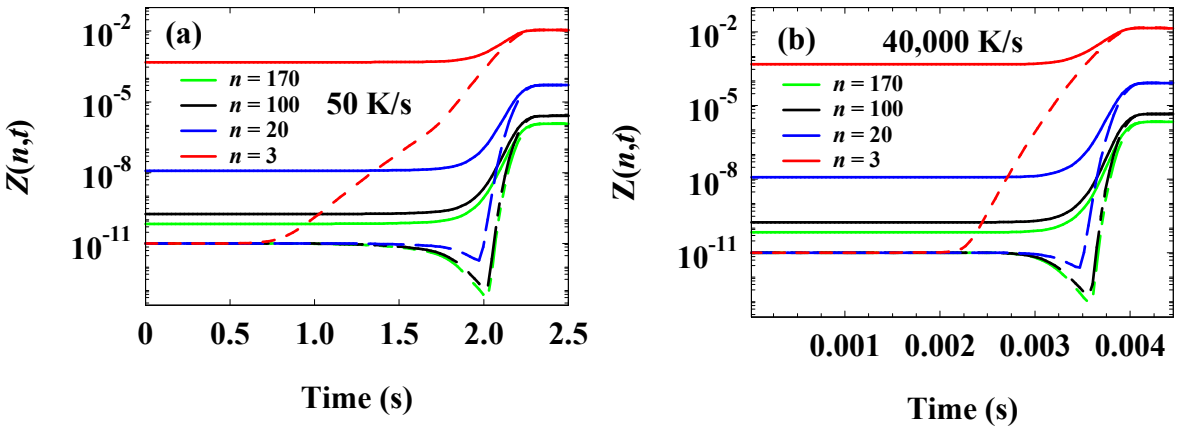

Figure 6 The calculated transient cluster densities for different initial cluster sizes as-deposited (Dashed lines), and pre-annealed (solid lines) at heating rates of (a) 50 K/s and (b) 40 000 K/s.

The pre-annealing simulations in this section produced the particular steady-state cluster size distribution in Figure 4(a), with narrow distributions of small and large clusters in the amorphous material. To study the effects of a wider range of non-uniform initial cluster size distributions on the crystallization dynamics in phase-change materials, theoretical Gaussian cluster size distributions with different monomer means, widths and densities will be implemented as initial states in the Master rate equation, and their impact on crystallization dynamics will be studied. These distributions can provide insight into the correlation between specific cluster size distributions and crystallization rates, and may guide the development of potential heat treatments that enhance the crystallization speeds in phase-change material for fast data processors and memories.

2.2.2. Theoretical cluster size distributions

The Gaussian distribution function is implemented here to describe theoretical distributions of pre-existing clusters $Z(n,0)$ in the amorphous parent phase, which is written as:

$$Z(n,0) = A_0 \exp(-(n-\mu)^2 / \nu^2) \tag{3}$$

where $n \geq 2$, A_0 is a factor for setting the required initial volume fraction of crystallized material, n is cluster size, μ is the cluster distribution mean with standard deviation ν. The monomer mean and standard deviation are chosen to provide various initial cluster size distributions, and A_0 is used to set the required initial crystalline volume fraction χ_0 from substituting (2) into (3) and solving to yield:

$$A_0 = \chi_0 Z_0 \Big/ \sum_{n=2}^{n_{\max}} n \exp\left(-(n-\mu)^2 / \nu^2\right)$$

A low initial crystalline volume fraction of χ_0 = 0.05 (5%) was used consistently throughout the forthcoming simulations, and ramped annealing with constant heating rates of 50 K/s and 40,000 K/s will be used for the crystallization simulations. Figure 7 illustrates the theoretical initial Gaussian cluster size distributions that will be used in this work, with narrow and wide distributions of small, medium-sized and large clusters (preserving the initial volume fraction at 5%).

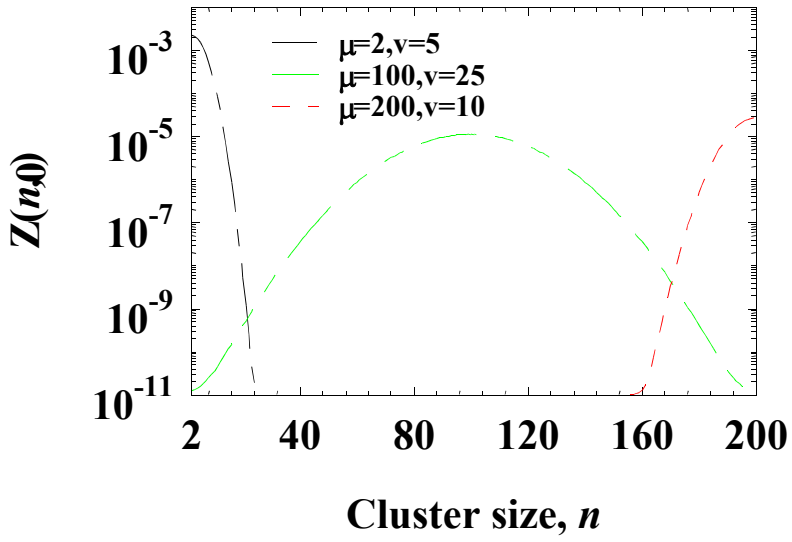

Figure 7 Gaussian distribution with different means and variances as labelled, providing different initial cluster size distributions with partial crystallization of 5% for the crystallization simulations in the Master rate equation.

Figure 8 shows the simulated crystalline volume fractions for the different initial amorphous states at different heating rates and compared to the as-deposited state. The figure shows general increase in initial crystalline fraction, reduction in the onset time for crystallization and in peak temperature due to the Gaussian initial cluster distributions in compared to the as-deposited state. These effects are more notable for the narrow distribution of small cluster sizes (black line when $\mu = 2$ and $\nu = 5$), while the wider distribution of larger cluster sizes (green line with $\mu = 100$) cause an early and slight increase in crystalline volume fraction but with a modest effect later on the crystallization temperature and time. When there is a narrow distribution of larger clusters only (red line with $\mu = 200$), the crystallization curve approaches that for the as-deposited initial state. This is true for both low (50 K/s) and high (40,000 K/s) heating rates. Figure 8(c) shows the extracted peak temperatures (from the time derivative of the crystallization curves - not shown here) for each of the simulations results in Figure 8(a) and Figure 8(b), demonstrating the decrease in peak temperature (and therefore crystallization time) with smaller cluster sizes.

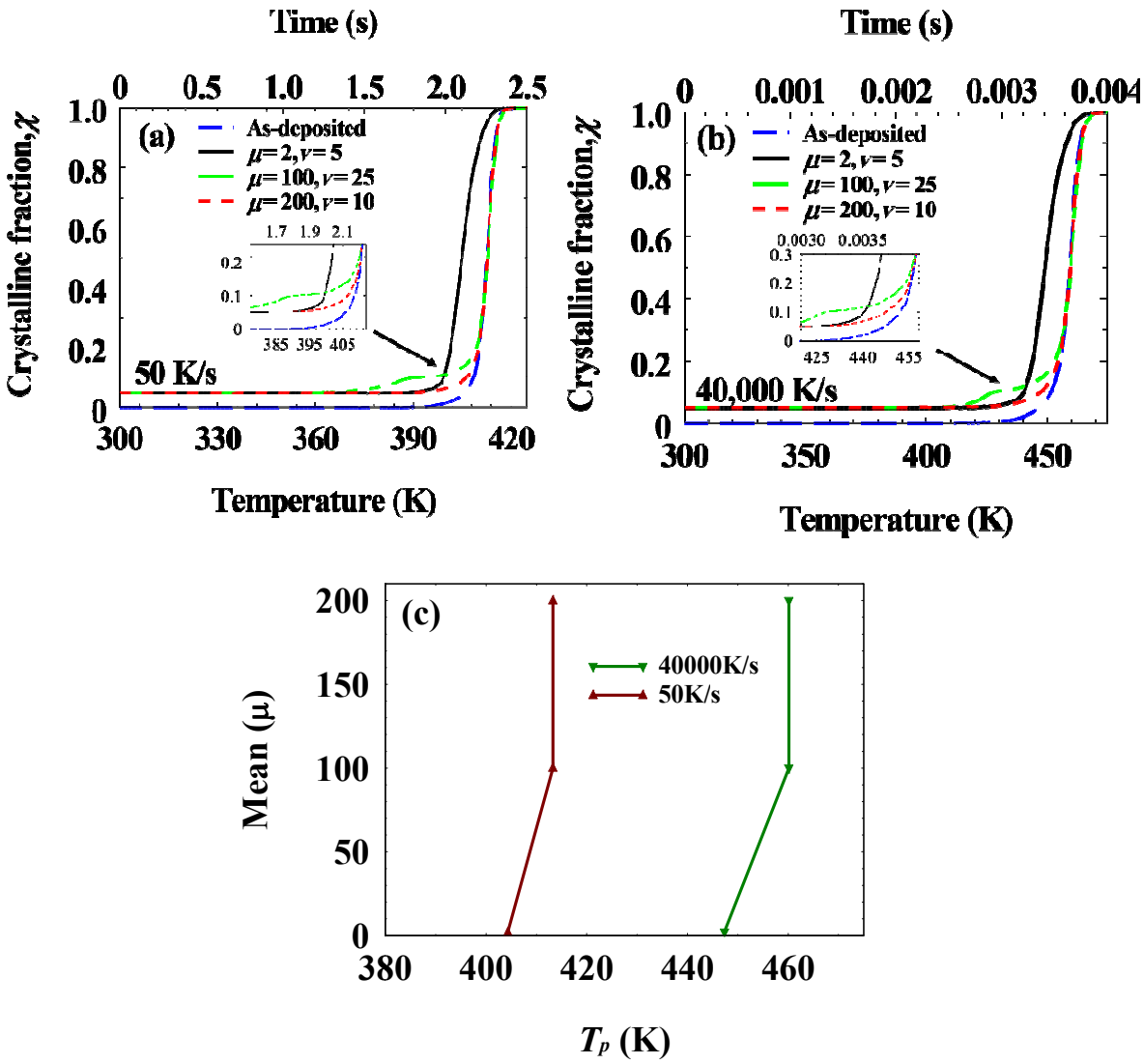

Figure 8 Calculated crystalline volume as a function of temperature during ramped anneals at two different heating rates with different Gaussian distribution as an initial state. (a) 50 K/s. (b) 40,000 K/s. (c) Extracted peak temperatures from (a) and (b).

The simulated transient cluster size distributions corresponding to the crystallization curves in Figure 8 are presented in Figure 9 for a selection of cluster sizes. For initial Gaussian distributions where small clusters are either absent (Figure 9(a) and (b) where μ = 200) or relatively low (Figure 9(c) and (d) with μ = 100), the larger clusters tend to dissociate and contribute to enhancing the growth of the smaller clusters, which require longer time to nucleate and grow. Both of these effects cause modest decreases in crystallization time and temperature, leading to crystallization curves approaching those produced with the as-deposited initial state. On the other hand, for the initial Gaussian distribution where the concentration of small clusters is high (Figure 9(e) and (f) with μ = 2), the abundance of smaller clusters enhances the formation and growth of larger

clusters leading to the marked decrease in crystallization time and temperature. The same crystallization trends are observed for the heating rates of 50 K/s (Figure 9(a), (c), and (e)) and 40,000 K/s (Figure 9(b), (d), and (f)).

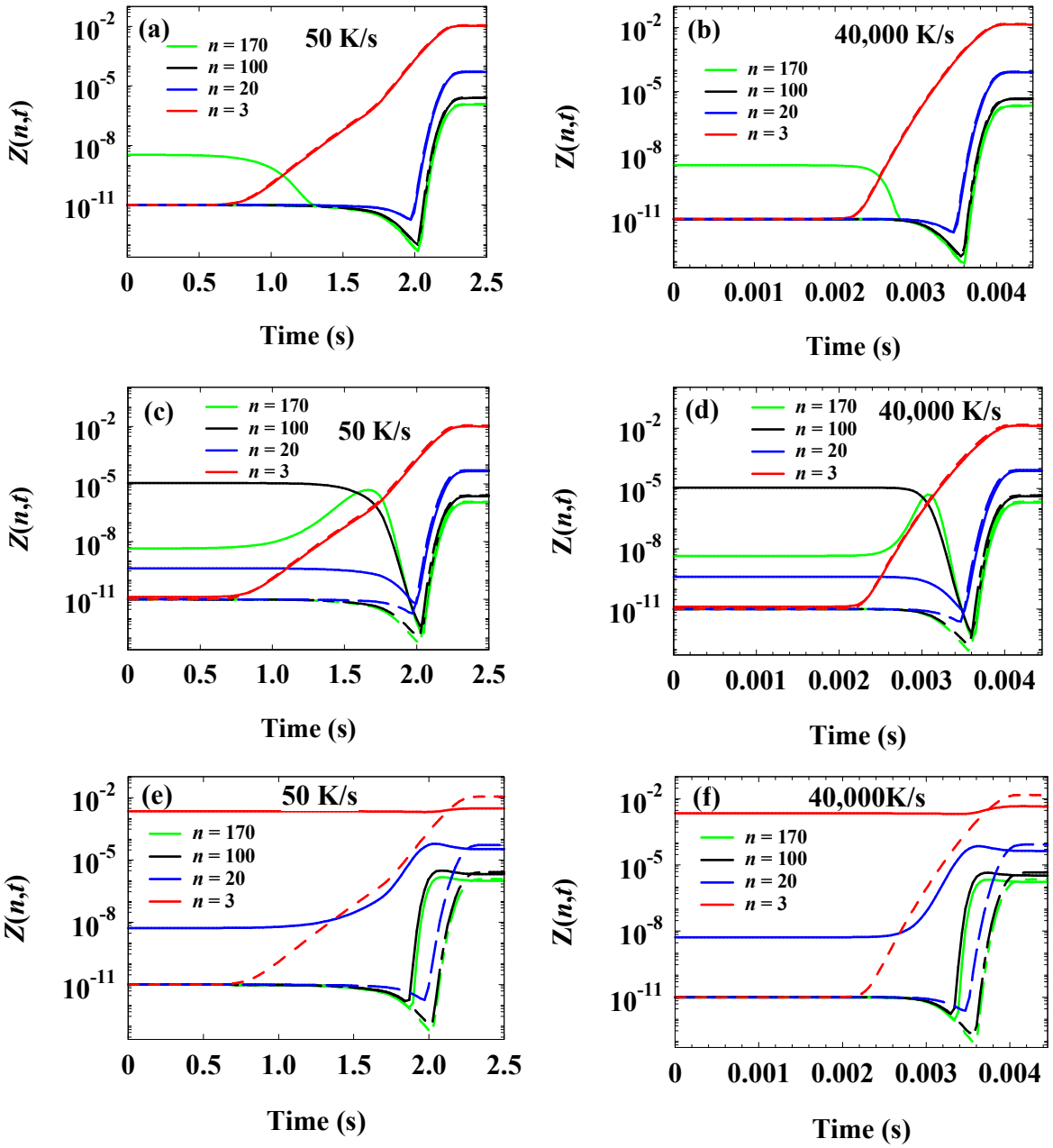

Figure 9 Simulated transient cluster densities for different initial cluster sizes: as-deposited (dashed lines), Gaussian cluster size distributions (solid lines) for (μ=200, ν=10) in (a) and (b), (μ=100, ν=25) in (c) and (d), and (μ=2, ν=5) in (e) and (f), at heating rates of 50 K/s and 40,000 K/s as labelled.

3. Conclusions

The Master rate equation approach was used in this work to investigate the influence of the size distribution of pre-existing crystalline clusters on the crystallization dynamics in phase-change materials. This was possible due to the ability of the Master rate equation in modelling and following the transient formation and growth of clusters of different sizes subject to a thermal history. This approach provided insight into the mechanisms of crystallization following different thermal treatments of phase-change materials, which is crucial to reduce the crystallization time and enhance the operating speeds of phase-change memories and data processors.

The three initial states simulated in this work included the as-deposited, melt-quenched and pre-annealed amorphous states, which normally result as part of the thermal treatment of phase-change materials in practical devices. The calculated steady-state cluster size distributions resulting from each of these states were then used as initial conditions for transient simulations of crystallization under ramped annealing at low and high heating rates. The simulations revealed that fast melt-quenching with cooling times of few nanoseconds produce a very narrow distribution of small nano-clusters, with similar crystallization dynamics to the as-deposited state following ramped annealing. Pre-annealing using ramped heating at low heating rates to temperatures lower than the crystallization temperature on the other hand produced a narrow distribution of nano-clusters up to 20 monomers in size, in good agreement with observations of formation of nano-clusters in the size range of 2-8 nm in sputtered and flash-evaporated GST using high resolution TEM. Simulations of crystallization using these initial cluster size distribution using the Master rate equation at low (50 K/s) and high (40,000 K/s) heating rates, revealed slight reduction in crystallization time and temperature compared to the as-deposited state. This was attributed to the large and narrow distribution of nano-clusters promoting the formation and growth of larger clusters and slightly enhancing crystallization. To examine in more detail the influence of a wider range of initial cluster size distributions on crystallization dynamics, theoretical Gaussian distributions were used as initial states in the Master rate equation, with controlled means and standard deviations but keeping the overall crystalline volume fraction constant at 5% in all cases. The subsequent crystallization simulations revealed a marked reduction in crystallization time

and temperature (and hence increased crystallization rate) when there is an abundance of only small nano-clusters embedded in the amorphous phase. The simulated transient cluster size distributions for the different cluster sizes showed that small clusters promote nucleation and growth of larger clusters and hence increase the crystallization rate, while large clusters tend to dissociate to help the formation of small clusters leading to crystallization curves that approach those produced from the as-deposited initial amorphous phase (which require longer times to nucleate and grow). Thus the simulations show that fast crystallization favours the priming of the amorphous phase to produce a large concentration of small clusters (less than 20 monomers).

References

[1] S. Raoux and M. Wuttig (Eds.), "*Phase-change Materials: Science and Applications*", Springer Science & Business Media (2010).
[2] C. D. Wright, Y. Liu, K. Kohary, M. M. Aziz, R. J. Hicken, Advanced Materials 23 (30), 3408 (2011).
[3] C. D. Wright, P. Hosseini, and J. A. Vazquez Diosdado, Advanced Functional Materials 23 (18), 2248 (2013).
[4] C. D. Wright, Nature Nanotechnology 11 (8), 655 (2016).
[5] F. Xiong, A. D. Liao, D. Estrada, and E. Pop, Science 332 (6029), 568 (2011).
[6] H. Hayat, K. Kohary, and C. D. Wright, Nanotechnology 28 (3), 35202 (2017).
[7] D. Loke, T. H. Lee, W. J. Wang, L. P. Shi, R. Zhao, Y. C. Yeo, T. C. Chong, and S. R. Elliott, Science 336 (6088), 1566 (2012).
[8] T. Nirschl et al., 2007 IEEE International Electron Devices Meeting, Washington, DC, 2007, pp. 461-464.
[9] C. F. Chen et al., 2009 IEEE International Memory Workshop, Monterey, CA, 2009, pp. 1-2.
[10] P. K. Khulbe, E. M. Wright, and M. Mansuripur, J. Appl. Phys. 88, 3926 (2000).
[11] S. Raoux, R. Shelby, B. Munoz, M. Hitzbleck, D. Krebs, M. Salinga, M. Woda, M. Austgen, K. M. Chung, and M. Wuttig, Eur. Phase Chang. Ovonic Sci. Symp., Prague 40 (2008).
[12] T. Wagner, J. Orava, J. Prikryl, T. Kohoutek, M. Bartos, and M. Frumar, Thin Solid Films 517, 4694 (2009).
[13] M. Frumar, T. Kohoutek, J. Prikryl, J. Orava, and T. Wagner, Phys. Status Solidi 246, 1871 (2009).
[14] B.-S. Lee, R. M. Shelby, S. Raoux, C. T. Retter, G. W. Burr, S. N. Bogle, K. Darmawikarta, S. G. Bishop, and J. R. Abelson, J. Appl. Phys. 115, 63506 (2014).
[15] D. Kashchiev, "*Nucleation: Basic Theory and Applications*", Butterworth-Heinemann, 2000.
[16] K. F. Kelton, J. Non. Cryst. Solids 163, 283 (1993).
[17] S. Senkader and C. D. Wright, J. Appl. Phys. 95, 504 (2004).
[18] A. Aladool, M. M. Aziz, and C. D. Wright, J. Appl. Phys. 121, 224504 (2017).
[19] J. Orava, L. L. Greer, B. Gholipour, D. W. W. Hewak, and C. E. E. Smith, Nature Materials 11, 279 (2012)
[20] B. Chen, J. Momand, P. A. Vermeulen, and B. J. Kooi, Cryst. Growth Des. 16, 242 (2016).
[21] K. B. Blyuss, P. Ashwin, A. P. Bassom, and C. D. Wright, Phys. Rev. E 72, 11607 (2005).
[22] N. Yamada, E. Ohno, K. Nishiuchi, N. Akahira, and M. Takao, J. Appl. Phys. 69, 2849 (1991).
[23] K. Kohary and C. D. Wright, Appl. Phys. Lett. 98, 223102 (2011).
[24] A. Sebastian, M. Le Gallo, and D. Krebs, Nat. Commun. 5, 1 (2014).
[25] E. Morales-Sánchez, E. F. Prokhorov, A. Mendoza-Galván, and J. González-Hernández, J. Appl. Phys. 91, 697 (2002).
[26] J. A. Kalb, M. Wuttig, and F. Spaepen, J. Mater. Res. 22, 748 (2007).
[27] J.-Y. Cho, D. Kim, Y.-J. Park, T.-Y. Yang, Y. Lee, and Y.-C. Joo, Acta Mater. 94, 143 (2015).
[28] J. Kalb, F. Spaepen, T. P. Leervad Pedersen, and M. Wuttig, J. Appl. Phys. 94, 4908 (2003).
[29] D.-H. Kim, F. Merget, M. Först, and H. Kurz, J. Appl. Phys. 101, 64512 (2007).
[30] B. J. Kooi, W. M. G. Groot, and J. T. M. De Hosson, J. Appl. Phys. 95, 924 (2004).